Supporting Information

Aggregation-Induced Electrochemiluminescence Bioconjugate of Apoferritin Encapsulated Iridium (III) Complexes for Biosensing Application

Lei Yang,[†] Xu Sun, [†] Dong Wei, [‡] Huangxian Ju, [†] Yu Du,*, [†] Hongmin Ma*, [†], and Qin Wei [†]

[†] Collaborative Innovation Center for Green Chemical Manufacturing and Accurate Detection, School of Chemistry and Chemical Engineering, University of Jinan, Jinan 250022, PR China.

[‡] School of Resources and Environment, University of Jinan, Jinan 250022, PR China.

* Corresponding author

Tel.: +86 531 82765730;

Fax: +86 531 82765969;

E-mail: duyu_ujn@163.com (Y. Du), mahongmin2002@126.com (H. M. Ma)

Contents:

S1. Materials, reagents and apparatus.

Graphite powder, gold chloride tetrahydrate ($HAuCl_4 \cdot 4H_2O$), horse spleen apoferritin (100 mg), bovine serum albumin (BSA) (96– 99%), 1-(3-(dimethylamino) propyl)-3-ethyl carbodiimide hydrochloride (EDC), and N-hydroxysuccinimide (NHS) were purchased from Sigma-Aldrich Co. (St. Louis, MO, USA). The *fac*-tris(2-phenylpyridine)iridium, and $FeCl_3$ $6H_2O$ were obtained from Shanghai Reagent Company (Shanghai, China). HWRGWVC heptapeptide (HWR) was ordered from GL Biochem. Ltd. (Shanghai, China). The capture-antibody (Ab_1), detection antibody (Ab_2) and antigen of CYFRA 21-1, antigens of PSA, PCT, CEA were all purchased from Shanghai Linc-Bio Science Co. LTD (Shanghai, China). All of the other chemicals were of analytical reagent grade and were used without further purification. Phosphate buffered saline (PBS) was prepared by using 0.1 M Na_2HPO_4 and 0.1 M KH_2PO_4 solution. 5 mM $K_3Fe(CN)_6/K_4Fe(CN)_6$ and 0.1 M KNO_3 solution were used as electrolyte for electrochemical impedance spectroscopy (EIS) and electro-active surface area study. Deionized water (18.25 MΩ/cm, 20 °C) was used for all the experiments.

Scanning electron microscope (SEM) images was obtained by a field emission SEM (Zeiss, Germany). Transmission electron microscope (TEM) and high resolution TEM (HRTEM) images were obtained by JEOL JEM-2100F (Japan). The D8 focus diffractometer (Bruker AXS, Germany) was used to complete the X-ray diffraction (XRD) patterns. Dynamic Light Scattering (DLS) was obtained from the Zetasizer Nano ZS 90 (Malvern, U.K.). ICP-OES tests were conducted by Agilent 720ES. Circular dichroism (CD) spectrum was obtained by Applied Photophysics. Ltd (Britain). The

ECL spectrum was obtained on a homemade ECL spectrum analyzer consisting of an Acton SP2300i mono-chromator equipped with a liquid N_2-cooled PyLoN 400BReXcelon digital charge-coupled device (CCD) detector (Princeton Instruments) and a VersaSTAT 3 electrochemical analyzer (Princeton Applied Research). The ECL measurements were performed with a MPI-F flow-injection ECL detector (Xi'an remax Electronic Science Tech. Co. Ltd., China) and electrochemical measurements were carried out on electrochemical workstation (Zahner Zennium PP211, Germany) using a three-electrode system which is made up of a platinum wire as an auxiliary electrode, an Ag/AgCl electrode as reference electrode, and GCE (4 mm in diameter) as working electrode.

S2. The DLS, CD, and ECL Measurements.

DLS experiments were performed on a Zetasizer Nano ZS90 (Malvern, U.K.) at 25 °C. The samples with a was diluted to a final concentration of 1.0 μM. Data were collected three times at 25 °C for each measurement.

The CD spectra were obtained by scanning from 200 to 300 nm utilizing a MOS-450 spectrometer consisting of a quartz cuvettes of 1 mm optical path length at 25 ^{o}C. All the data were expressed in terms of mean residual ellipticity (h) in deg cm^2 $dmol^{-1}$.

All the ECL measurements were conducted by the MPI-F ECL analyzer in 10 mL of PBS (pH 7.4), where the photomultiplier voltage was set at 700 V. The cyclic voltammetry test was conducted on the electrochemical workstation by scanning the biosensor positively from 0 to 1.2 V with a scanning rate of 100 mV/s.

S3. SEM image of pure Fe_2N/rGO

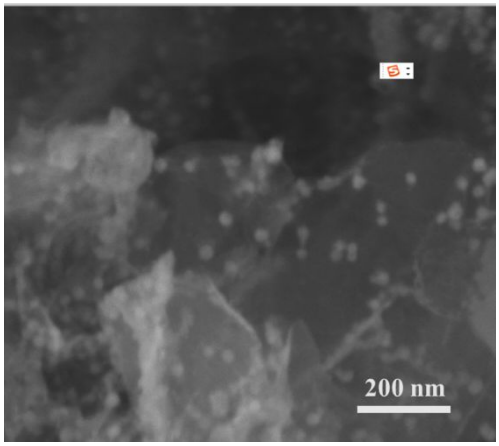

Figure S1. SEM image of Fe_2N/rGO composites.

S4. Elemental mapping of Fe_2N/rGO/Au composite

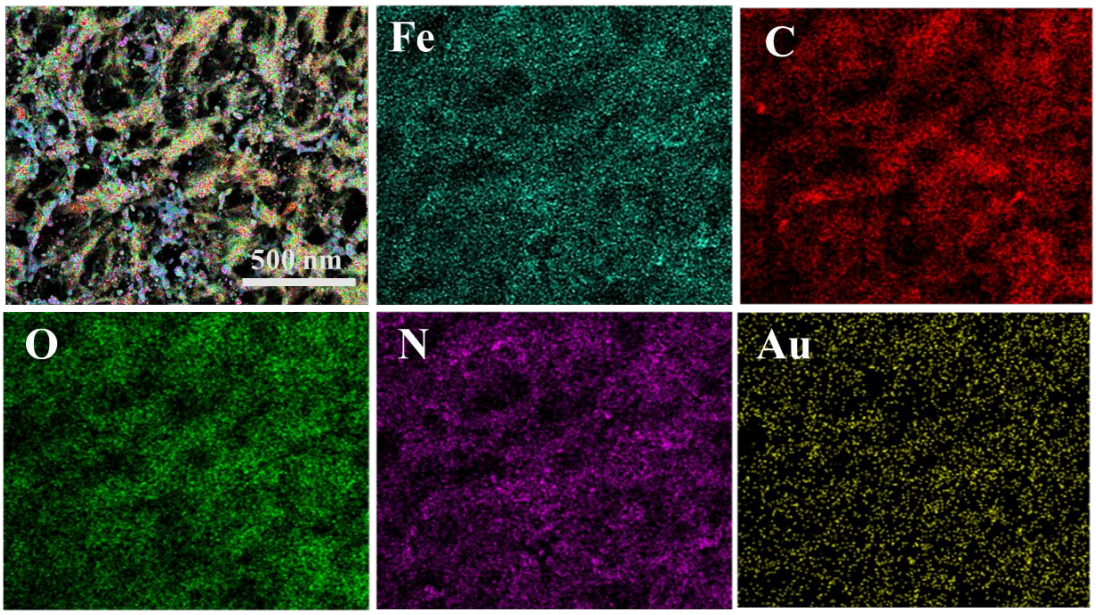

Figure S2. Elemental mapping of Fe_2N/rGO/Au composites.

S5. TEM image of pure apoFt and DLS of $Ir(ppy)_3$ aggregates

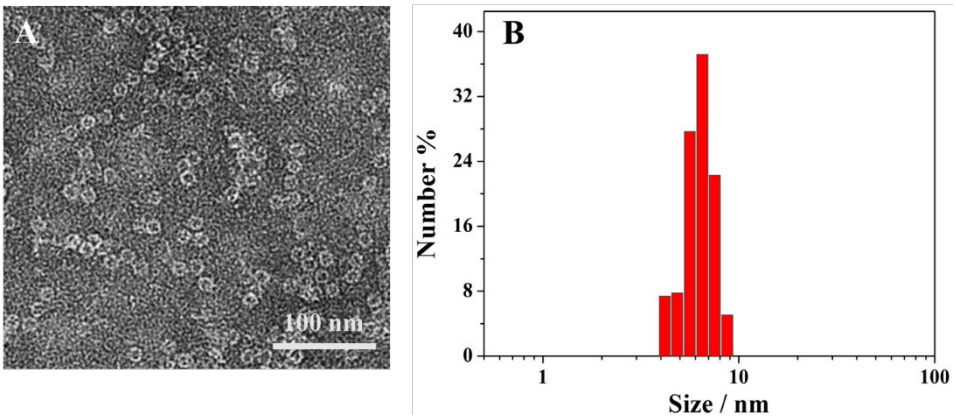

Figure S3. TEM image of pure apoFt (A) and size distribution (B) of $Ir(ppy)_3$ aggregates by DLS.

The pure $Ir(ppy)_3$ aggregates were released from the apoFt cavity by disassociating the apoFt subunits at pH 10.8. In details, the pH value of 2 mL of $Ir(ppy)_3$@apoFt solution (5 mg/mL) was adjusted to 10.8 by the addition of sodium hydroxide (0.1 mol/L). After stirring for 2 h to fully disassociate the apoFt subunits, and the released $Ir(ppy)_3$ self-assemblies were collected by three times of ultrafiltration (Amicon Ultra- 4 mL 10 KDa, Millipore) and dispersed into 2 mL of solution.

S6. Catalyzed oxidation of TPrA by Fe_2N/rGO/Au composite.

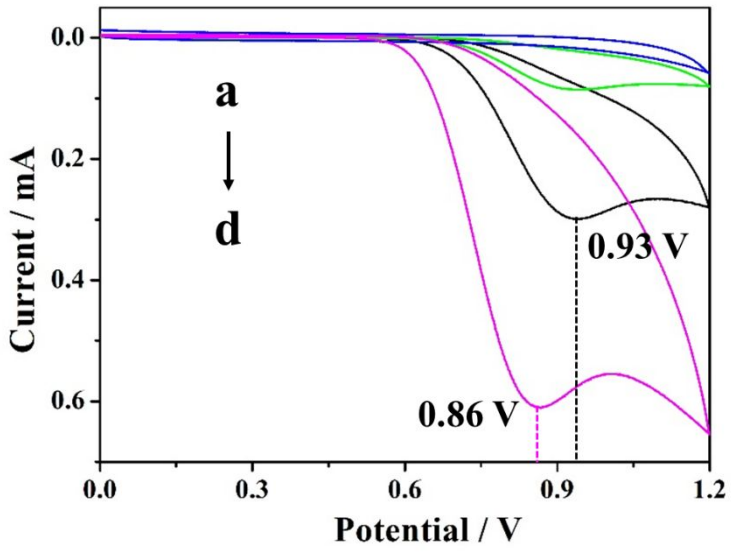

Figure S4. CV curves of bare GCE detected in 10 mL of PBS (0.1 mol/L, pH 7.4) without TPrA (a) and with 25 mmol/L of TPrA (b), Fe_2N/rGO/Au modified GCE in 10 mL of PBS (0.1 mol/L, pH 7.4) without TPrA (c) and with 25 mmol/L of TPrA (d).

S7. ICP-OES calibration curve.

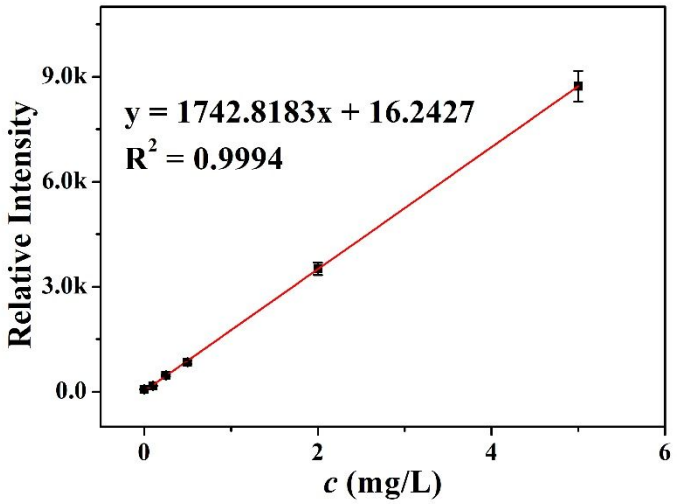

Figure S5. ICP-OES calibration curve of standard Ir samples.

S8. Intra-assay of pH-induced encapsulation of $Ir(ppy)_3$ in apoFt

To investigate the reproducibility of the proposed pH-induced encapsulation method, intra-assay was further conducted. The Ir contents of of $Ir(ppy)_3$@apoFt samples (1 mL, 25 mg/mL) of different batches were quantified by using ICP-OES. All the $Ir(ppy)_3$@apoFt samples were 125 times diluted and then 5 mL of diluted samples (0.2 mg/mL) were used for the ICP-OES analysis.

Table S1. The Ir contents of $Ir(ppy)_3$@apoFt samples of different batches

Batch number	ICP-OES intensity	Instrument reading *C* (μg /mL)	Volume (mL)	Ir contents (μg/mg)	Encapsulation number of $Ir(ppy)_3$	RSD (%)	Mean number
1	6604.09	3.78		18.90	45.27		
2	6150.96	3.52		17.60	42.17		
3	5959.25	3.41	5	17.05	40.88	5.99	44.32
4	6778.37	3.88		19.40	46.47		
5	6830.66	3.91		19.55	46.83		

S9. PL spectra of $Ir(ppy)_3$ aggregates and monomers.

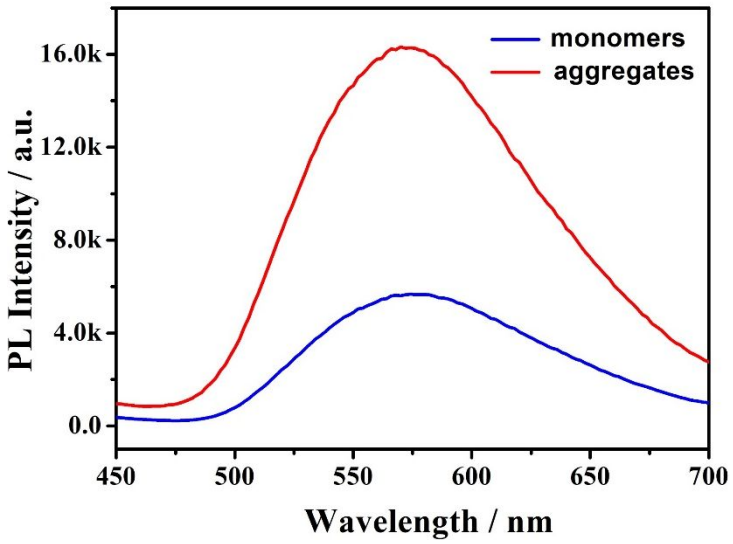

Figure S6. PL spectra of *sample A* (red curve) and *sample B* (blue curve).

S10. EIS characterization for immunosensor assembly

Stepwise characterization of the proposed biosensor was confirmed with EIS and CV profiles conducted in $[Fe(CN)_6]^{4-/3-}$ (5 mmol/L) solution containing KCl (0.1 mol/L). Impedance spectra of GCE at different modified steps was shown in Figure S7. The charge transfer resistance (R_{ct}) data of GCE/Fe_2N/rGO/Au-HWR (curve b) only slightly increased as compared to the bare GCE (curve a), proving the good electrical conductivity of Fe_2N/rGO/Au because HWR as a peptide can hinder the electro transfer. After the continuous modifications of nonconductive BSA, Ab_1, Ag and $Ir(ppy)_3$@apoFt-Ab_2 on the GCE surface, R_{ct} data (curve c, d, e, and f) increased sequentially due to their poor conductivity of proteins, indicating the superficial construction of the proposed ECL immunoosensor was successful.

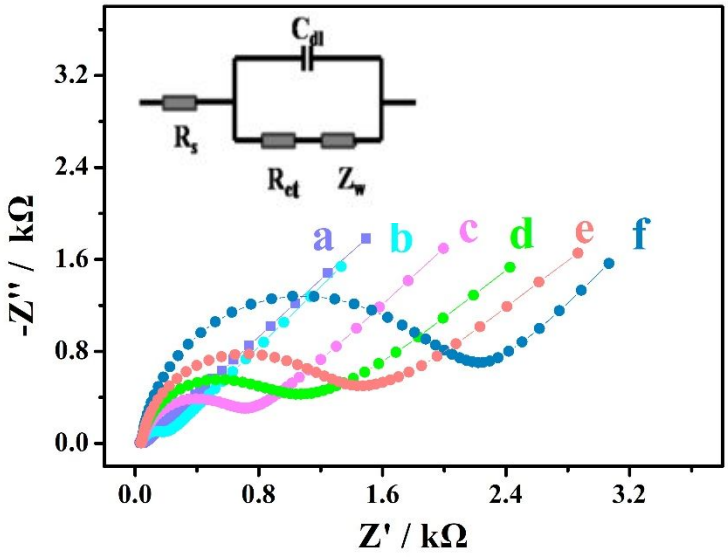

Figure S7. EIS characterization of the stepwise characterization of the proposed immunosensor.

S11. Optimization of experimental conditions

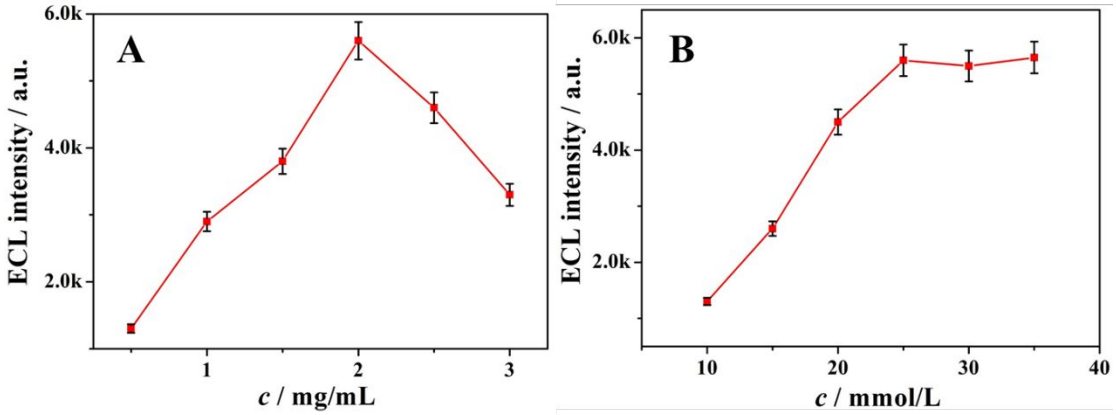

Figure S8. Optimizations of the (A) Fe_2N/rGO/Au concentration and TPrA concentration (B).

Optimizing the experimental conditions is crucial for achieving satisfying ECL performances. At the beginning, PBS with pH value of 7.4 was used throughout in this work to maintain the biological activity of biomolecules. Then, the concentration of Fe_2N/rGO/Au substrates was optimized since the piled Fe_2N/rGO/Au composites on GCE might block the electron transfer between electrode surface and electrolyte. As shown in Figure S8A, it is clearly seen that the maximum ECL intensity appeared at 2 mg/mL, thus making it the optimized concentration for Fe_2N/rGO/Au composite. As the essential partner of the ECL emission of $Ir(ppy)_3$, the TPrA concentration was also optimized for better ECL performance. As shown in Figure S8B, the maximum ECL intensity reached at 25 mmol/L. Therefore, the concentration of TPrA was optimized to be 25 mmol/L in this work.

S12. Specificity, stability and reproducibility of the immunosensor

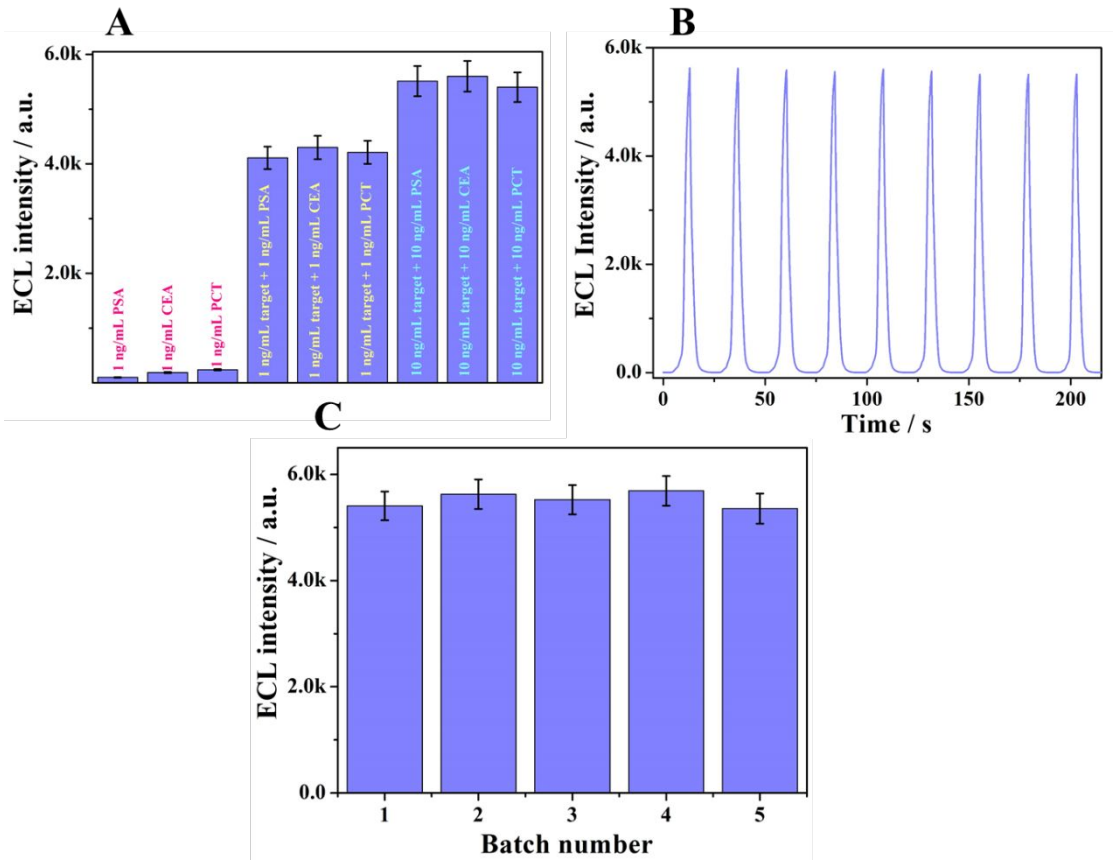

Figure S9. (A) Specificity of the proposed ECL immunosensor. (B) Stability of the immunosensor. (C) Reproducibility of same electrode in five different batches (C). Error bars, SD, n = 5.

To evaluate the specificity of the immunosensor for CYFRA 21-1 detection, three representative interfering proteins (1 ng/mL) in human serum including CEA, PCT, and PSA were detected. In Figure S9A, ECL immunosensors incubated with interferences (1 ng/mL) showed negligible influences. Meanwhile, immunosensors incubated with mixed samples (1 ng/mL of CYFRA 21-1 + 1 ng/mL of interferences and 10 ng/mL of CYFRA 21-1 + 10 ng/mL of interferences) also showed slight changes with RSD of

3.25% and 4.56%, suggesting the good specificity of the proposed immunosensor. In Figure S9B, operating stability was investigated by scanning the electrodes incubated with 10 ng/mL of for 9 cycles, where the ECL intensities were found with no significant changes with RSD of 1.45%, illustrating that the good stability of the proposed immunosensor. Reproducibility of the immunosensor was inspected by measuring same ECL biosensors incubated with 10 ng/mL of CYFRA 21-1 in five different batches (Figure S9C), and the sensors were constructed by different operators and measured by different ECL analyzers. With an acceptable RSD of 4.24%, the good reproducibility of proposed ECL biosensor was also proved.

S13. Comparison of the proposed method with other reported methods

Table S2. Comparison of the proposed method with other reported methods

Electrode materials	Linear range (ng/mL)	Detection limit (pg/mL)	Ref
3D graphene-Au NPs	0.25 — 800	100	1
CeO_2 nanocube/RGO	6.25×10^{-4} — 0.01	0.625	2
ZrO_2-RGO	2 — 22	122	3
Fe_2N/rGO/Au+ $Ir(ppy)_3$@apoFt	1×10^{-3} — 50	0.43	this work

Reference

(1) Zeng, Y.; Bao, J.; Zhao, Y.; Huo, D.; Chen, M.; Yang, M.; Fa, H.; Hou, C., A Sensitive Label-free Electrochemical Immunosensor for Detection of Cytokeratin 19 Fragment Antigen 21-1 Based on 3D Graphene with Gold Nanopaticle Modified Electrode. *Talanta* **2018,** *178*, 122–128.

(2) Pachauri, N.; Dave, K.; Dinda, A.; Solanki, P. R., Cubic CeO_2 Implanted Reduced Graphene Oxide-Based Highly Sensitive Biosensor for Non–Invasive Oral Cancer Biomarker Detection. *J. Mater. Chem. B.*

2018, *6,* 3000.

(3) Kumar, S.; Sharma, J. G.; Maji, S.; Malhotra, B. D. Nanostructured Zirconia Decorated Reduced Graphene Oxide Based Efficient Biosensing Platform for Non–Invasive Oral Cancer Detection. *Biosens. Bioelectron.* **2016**, *78*, 497–504.